Predicting PML Performance at Normal Incidence in Cylindrical FDTD

Mohammed F. Hadi and Atef Z. Elsherbeni
Electrical Engineering, Colorado School of Mines, Golden, CO, USA

***Abstract*—The main objective of this presentation is to apply discrete FDTD theory to the stretched-coordinates PML for cylindrical FDTD and derive the overall numerical reflection coefficient off the PML region as a function of all algorithmic parameters and harmonic solutions. For brevity, analysis are limited to normal incidence on the radially arrayed PML region. Obtained predictive equations are used to investigate PML absorption as a function of cylindrical harmonics and proximity to the axis of rotation.**

I. Stretched-Coordinates PML Equations

To effect absorbing boundary conditions, the coordinate stretching variable [1] $s(\rho,\omega) = 1 + \frac{\sigma(\rho)}{\jmath\omega\epsilon}$ is used within the radial PML region which causes the stretched radial dimension

$$\bar{\rho}(\rho,\omega) = \rho_0 + \int_{\rho_0}^{\rho} s(\rho',\omega)d\rho' = \rho + \frac{d(\rho)}{\jmath\omega\epsilon}, \tag{1}$$

where ρ_0 is the innermost PML interface position from the z-axis. The parameter $\sigma(\rho)$ is graded for a smooth and reflections-free absorption of outgoing waves. The corresponding Maxwell's equations, when reduced for normal wave incidence-only TE^z analysis can be written as

$$\begin{aligned}
\jmath\omega\epsilon\bar{\rho}E_\rho &= \frac{\partial H_z}{\partial\phi} && (2)\\
\jmath\omega\epsilon s E_\phi &= -\frac{\partial H_z}{\partial\rho} && (3)\\
-\jmath\omega\mu s\bar{H}_z &= \frac{\partial\bar{E}_\phi}{\partial\rho} - \frac{\partial(sE_\rho)}{\partial\phi}, && (4)
\end{aligned}$$

with $\bar{E}_\phi = \bar{\rho}E_\phi$ and $\bar{H}_z = \bar{\rho}H_z$. Conversion to FDTD is accomplished using

$$\begin{aligned}
\jmath\omega sX &\rightarrow \frac{A_i^+ X|_i^{n+\frac{1}{2}} - A_i^- X|_i^{n-\frac{1}{2}}}{\Delta t}, && (5)\\
&\quad \text{for} \quad X \equiv E_\phi, \bar{H}_z\\
\jmath\omega\bar{\rho}E_\rho &\rightarrow \frac{B_i^+ E_\rho|_i^{n+\frac{1}{2}} - B_i^- E_\rho|_i^{n-\frac{1}{2}}}{\Delta t} && (6)
\end{aligned}$$

where $A_i^\pm = 1 \pm \Delta t\sigma_i/(2\epsilon)$, $B_i^\pm = \rho_i \pm \Delta t d_i/(2\epsilon)$, i, n are index counters along ρ, t,

$$\begin{aligned}
X_s|_i^{n+1} &= X_s|_i^n + \Delta t X|_i^{n+1} && (7)\\
Y|_i^{n+1} &= \bar{X}|_i^{n+1} + e^{-\Delta t/\tau_i} Y|_i^n && (8)\\
\rho_i X|_i^{n+1} &= \bar{X}|_i^{n+1} - \left(1 - e^{-\Delta t/\tau_i}\right) Y|_i^{n+1}, && (9)
\end{aligned}$$

and $\tau_i = \epsilon\rho_i/d_i$. Equations (7)–(9) are the recursive versions of the $s(t) * X(t)$ and $\bar{X}(t) * 1/\bar{\rho}(t)$ time convolutions.

II. Reduction to Radial-Only Finite Differences

The above time domain update equations need to be reduced to a single pair of equations in preparation for multi-layer reflection analysis [2]. This can be accomplished through embedding the ϕ and t finite differences with the TE^z harmonic solutions [3]

$$\begin{aligned}
F_z &= H_m^{(2)}(\beta\bar{\rho})e^{\jmath(\omega t - m\phi)} && (10)\\
E_\rho &= -\frac{1}{\bar{\rho}}\frac{\partial F_z}{\partial\phi} = \frac{\jmath m}{\bar{\rho}} H_m^{(2)}(\beta\bar{\rho})e^{\jmath(\omega t - m\phi)} && (11)\\
E_\phi &= \frac{\partial F_z}{\partial\bar{\rho}} = \beta H_m^{\prime(2)}(\beta\bar{\rho})e^{\jmath(\omega t - m\phi)} && (12)\\
H_z &= \frac{\beta^2}{\jmath\omega\mu} F_z = \frac{\beta}{\jmath\eta} H_m^{(2)}(\beta\bar{\rho})e^{\jmath(\omega t - m\phi)}. && (13)
\end{aligned}$$

This process is best done sequentially. Starting with time embedding in (7)–(9), we can solve for the auxiliary variables

$$\begin{aligned}
X_s|_i &= \frac{\Delta t}{1 - e^{-\jmath\omega\Delta t}} X|_i && (14)\\
\bar{X}|_i &= \frac{e^{\Delta t/\tau_i} - e^{-\jmath\omega\Delta t}}{1 - e^{-\jmath\omega\Delta t}}\ \rho_i X|_i \ = \ \bar{b}_i X|_i. && (15)
\end{aligned}$$

Completing the time dependence infusion, as well as ϕ embedding reduces the update equations to

$$\begin{aligned}
\epsilon D_t^B E_{\rho o} &= D_\phi H_{zo} && (16)\\
\epsilon D_t^A E_{\phi o} &= -\frac{\partial H_{zo}}{\partial\rho} && (17)\\
-\mu\bar{b}_i D_t^A H_{zo} &= \frac{\partial(\bar{b}_i E_{\phi o})}{\partial\rho} - K_i D_\phi E_{\rho o}, && (18)
\end{aligned}$$

where

$$\begin{aligned}
D_t^A &= \frac{A_i^+ e^{\jmath\omega\Delta t/2} - A_i^- e^{-\jmath\omega\Delta t/2}}{\Delta t} && (19)\\
D_t^B &= \frac{B_i^+ e^{\jmath\omega\Delta t/2} - B_i^- e^{-\jmath\omega\Delta t/2}}{\Delta t} && (20)\\
D_\phi &= -\jmath\frac{\sin(m\Delta\phi/2)}{\Delta\phi/2} && (21)\\
K_i &= 1 + \frac{\sigma_i\Delta t/\epsilon}{1 - e^{-\jmath\omega\Delta t}}. && (22)
\end{aligned}$$

Eliminating $E_{\rho o}$ finally produces

$$\begin{aligned}
\gamma_{Ei}\bar{b}_i E_{\phi o}|_i &= -\frac{H_{zo}|_{i+\frac{1}{2}} - H_{zo}|_{i-\frac{1}{2}}}{\Delta\rho} && (23)\\
-\gamma_{Hi} H_{zo}|_i &= \frac{\bar{b}_{i+\frac{1}{2}} E_{\phi o}|_{i+\frac{1}{2}} - \bar{b}_{i-\frac{1}{2}} E_{\phi o}|_{i-\frac{1}{2}}}{\Delta\rho}, && (24)
\end{aligned}$$

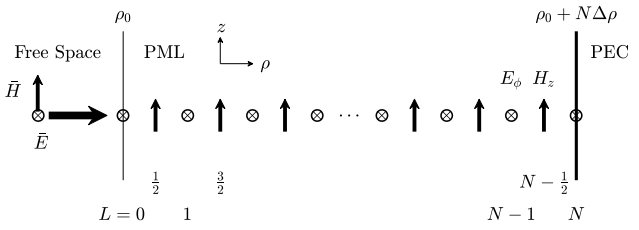

Fig. 1. A cylindrical wave impinging normally on a radially graded PML region.

respectively, where

$$\gamma_{Ei} = \frac{\epsilon D_t^A}{\bar{b}_i} \quad \text{and} \quad \gamma_{Hi} = \mu \bar{b}_i D_t^A - K_i \frac{D_\phi^2}{\epsilon D_t^B}. \tag{25}$$

III. Stretched-PML Reflection Coefficient

Fig. 1 shows (E_ϕ, H_z) field node distribution along the radial dimension within the PML layers, where the inner-most PML interface and the outer PEC backing coincide with E_ϕ field nodes. $E_{\phi o}$ and H_{zo} are now expressed as

$$E_{\phi o}|_L = \begin{cases} \tilde{\beta}_0 \left[H_m^{'(2)}(\tilde{\beta}_0 \rho_0) + \Gamma H_m^{'(1)}(\tilde{\beta}_0 \rho_0) \right], L = 0 \\ \tilde{\beta}_0 T_L, \quad L = 1, 2, \ldots, N-1 \\ 0, \quad L = N \end{cases} \tag{26}$$

$$H_{zo}|_L = \begin{cases} \frac{1}{j\eta} \tilde{\beta}_{-\frac{1}{2}} \\ \cdot \left[H_m^{(2)}(\tilde{\beta}_{-\frac{1}{2}} \rho_{-\frac{1}{2}}) + \Gamma H_m^{(1)}(\tilde{\beta}_{-\frac{1}{2}} \rho_{-\frac{1}{2}}) \right], L = -\frac{1}{2} \\ \frac{1}{j\eta} \tilde{\beta}_{-\frac{1}{2}} T_L, \quad L = \frac{1}{2}, \frac{3}{2}, \ldots, N-\frac{1}{2} \end{cases} \tag{27}$$

where Γ is the overall PML reflection coefficient and T_L lumps several inter-layer multi-reflection coefficients [4].

Populating (23)–(24) with these expressions, in a similar manner to [2], [4] ultimately produces the tridiagonal matrix equation $\mathbf{UT} = \mathbf{V}$, where

$$\mathbf{U} = \begin{bmatrix} U_0 & G_0 & & & & & \\ U_{\frac{1}{2}} & 1 & S_{\frac{1}{2}} & & & & \\ & -G_1 & 1 & G_1 & & & \\ & & & \ddots & & & \\ & & & -G_{N-1} & 1 & G_{N-1} & \\ & & & & -S_{N-\frac{1}{2}} & 1 & \end{bmatrix} \tag{28}$$

$$\mathbf{T} = \begin{bmatrix} \Gamma & \bar{T}_{\frac{1}{2}} & \bar{T}_1 & \cdots & \bar{T}_{N-1} & \bar{T}_{N-\frac{1}{2}} \end{bmatrix}^T \tag{29}$$

$$\mathbf{V} = \begin{bmatrix} V_0 & V_{\frac{1}{2}} & 0 & \cdots & 0 & 0 \end{bmatrix}^T \tag{30}$$

where

$$\bar{T}_L = \begin{cases} \bar{b}_L \tilde{\beta}_0 T_L, & L = 1, 2, \ldots, N-1 \\ -j\tilde{\beta}_{-\frac{1}{2}} T_L, & L = \frac{1}{2}, \frac{3}{2}, \ldots, N-\frac{1}{2} \end{cases} \tag{31}$$

$$S_L = \frac{\eta}{\Delta\rho \gamma_{HL}}, \; L = \frac{1}{2}, \frac{3}{2}, \ldots, N-\frac{1}{2} \tag{32}$$

$$G_L = \frac{1}{\eta \Delta\rho \gamma_{EL}}, \; L = 0, 1, \ldots, N-1 \tag{33}$$

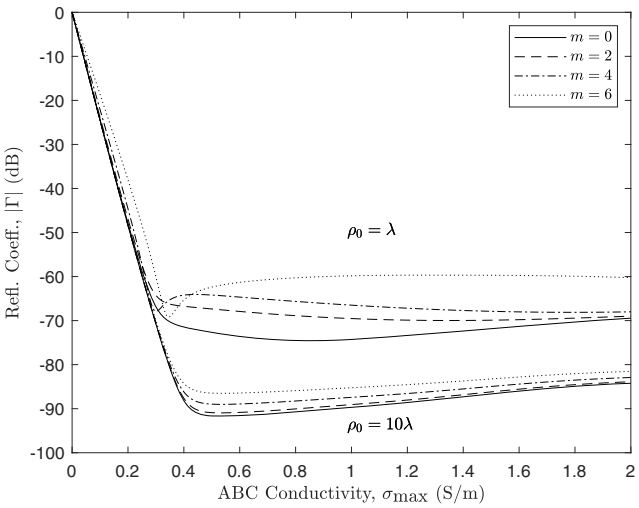

Fig. 2. Effect of PML proximity to the z-axis and harmonic order on PML performance. $f = 1$ GHz, $\Delta\rho = \Delta z = \lambda/R$, $\Delta\phi \simeq \Delta\rho/\rho_0$, $R = 20$ cells per wavelength, and cubic loss profile used.

$$U_0 = j\tilde{\beta}_{-\frac{1}{2}} G_0 H_m^{(1)}(\tilde{\beta}_{-\frac{1}{2}} \rho_{-\frac{1}{2}}) + \tilde{\beta}_0 \rho_0 H_m^{'(1)}(\tilde{\beta}_0 \rho_0) \tag{34}$$

$$V_0 = -j\tilde{\beta}_{-\frac{1}{2}} G_0 H_m^{(2)}(\tilde{\beta}_{-\frac{1}{2}} \rho_{-\frac{1}{2}}) - \tilde{\beta}_0 \rho_0 H_m^{'(2)}(\tilde{\beta}_0 \rho_0) \tag{35}$$

$$U_{\frac{1}{2}} = -\tilde{\beta}_0 \rho_0 S_{\frac{1}{2}} H_m^{'(1)}(\tilde{\beta}_0 \rho_0) \tag{36}$$

$$V_{\frac{1}{2}} = \tilde{\beta}_0 \rho_0 S_{\frac{1}{2}} H_m^{'(2)}(\tilde{\beta}_0 \rho_0). \tag{37}$$

The numerical wavenumber $\tilde{\beta}$ is obtained through solving the cylindrical FDTD numerical dispersion relation [5].

Fig. 2 is a typical outcome from this efficient reflections prediction. It compares Γ at different cylindrical harmonics (m) and $\rho_0 = \lambda, 10\lambda$. It is clear from the figure that as the PML region's position move further away from the z-axis, more and more harmonics are absorbed at the same level of $m = 0$ absorption. On the other hand, harmonic absorption degrades when the PML is brought closer to the z-axis, and this degradation increases with mode order. More analysis along with validating simulations will be presented during the conference.

References

[1] F. L. Teixeira and W. C. Chew, "PML-FDTD in cylindrical and spherical grids," *IEEE Microwave Guided Wave Lett.*, vol. 7, no. 9, pp. 285–287, Sep. 1997.

[2] M. F. Hadi, A. Z. Elsherbeni, R. C. Bollimuntha, and M. J. Piket-May, "Predicting near-field performance for the stretched-coordinates PML absorbing boundary conditions in spherical FDTD (submitted)," *IEEE Trans. Antennas Propagat.*, 2018.

[3] R. F. Harrington, *Time-Harmonic Electromagnetic Fields*. Ney York, NY: McGraw-Hill, 1961.

[4] M. F. Hadi, "Near-field PML optimization for low and high order FDTD algorithms using closed-form predictive equations," *IEEE Trans. Antennas Propagat.*, vol. 59, no. 8, pp. 2933–2942, Aug. 2011.

[5] M. F. Hadi and A. Z. Elsherbeni, "Numerical dispersion and stability for three-dimensional cylindrical FDTD near the axis of rotation," in *11th European Conference on Antennas and Propagation*, Paris, France, Mar. 2017, pp. 936–938.